A synergistic action of sirtuins directly recognizes DNA breaks and potentiates DNA damage response and repair

Fanbiao Meng,[1,2,9] Minxian Qian,[1,3,5,9] Bin Peng,[1,9] Xiaohui Wang,[1,6] Linyuan Peng,[1,3,5] Kang Zheng,[7] Zuojun Liu,[1,3,5] Xiaolong Tang,[1,3,5] Shuju Zhang,[1] Shimin Sun,[1,7] Xinyue Cao,[1,3,5] Qiuxiang Pang,[7] Bosheng Zhao,[7] Wenbin Ma,[8] Zhou Songyang,[8] Bo Xu,[2] Wei-Guo Zhu,[1,5,6] Xingzhi Xu,[1,6*] Baohua Liu[1,3,4,5,6*]

[1]Guangdong Key Laboratory of Genome Stability and Human Disease Prevention, School of Basic Medical Sciences, Shenzhen University, Shenzhen 518055, China

[2]The Key Laboratory of Breast Cancer Prevention and Therapy, Ministry of Education, Tianjin's Clinical Research Center for Cancer, Tianjin Medical University Cancer Institute and Hospital, National Clinical Research Center for Cancer, Tianjin 300006, China

[3]Shenzhen Key Laboratory for Systemic Aging and Intervention, National Engineering Research Center for Biotechnology (Shenzhen), Shenzhen University Health Science Center, Shenzhen 518055, China

[4]Guangdong Provincial Key Laboratory of Regional Immunity and Diseases, School of Basic Medical Sciences, Shenzhen University Health Science Center, Shenzhen 518055, China

[5]Department of Biochemistry & Molecular Biology, School of Basic Medical Sciences, Shenzhen University, Shenzhen 518060, China

[6]Carson International Cancer Center, Shenzhen University Health Science Center, Shenzhen 518055, China

[7]Anti-aging & Regenerative Medicine Research Institution, School of Life Sciences, Shandong University of Technology, Zibo 255049, China

[8]Key Laboratory of Gene Engineering of the Ministry of Education and State Key Laboratory for Biocontrol, School of Life Sciences, Sun Yat-sen University, Guangzhou, China

[9]These authors contribute equally to this work.

* Correspondence should be addressed to Dr Baohua Liu (ppliew@szu.edu.cn)

Summary

DNA damage response (DDR) is a highly orchestrated process; initially how the DNA breaks are recognized need in-depth study. Here, we show that polymerized SIRT6 deacetylase recognizes double-strand DNA breaks (DSBs) and potentiates DDR. SIRT1 deacetylates SIRT6 at residue K33, which is important for SIRT6 polymerization and mobilization toward DNA breaks. The K33-deacetylated SIRT6 anchors to γH2AX, allowing its retention on and subsequent remodeling of local chromatin. The K33R mutation, mimicking hypoacetylated SIRT6, rescues defective DNA repair imposed by *SIRT1* deficiency in cells. Our data highlights a synergistic action of SIRTs in spatiotemporal regulation of DDR and DNA repair.

Key Words: SIRT1, SIRT6, DNA damage response (DDR), deacetylation

Introduction

DNA damages are frequently induced by a variety of endogenous and exogenous agents. DNA damage response (DDR) is immediately elicited to ensure the genomic integrity, which is initiated by DNA break recognition, then followed by chromatin remodeling, signaling transduction and amplification (1). Double-strand breaks (DSBs) represent the most severe form of DNA lesions, recognized by the Mre11-Rad50-Nbs1 (MRN) complex, which recruits and activates phosphatidylinositol 3-kinase-like protein kinase ataxia-telangiectasia mutated (ATM) or ATM- and Rad3-related (ATR). H2AX is then rapidly phosphorylated (γH2AX) by ATM/ATR, serving as a platform to orchestrate repair proteins to the vicinity of DNA breaks (2). Simultaneously, a variety of histone-modifying enzymes, heterochromatin factors and ATP-dependent chromatin remodelers cooperatively create a relaxed chromatin structure, allowing the access of additional repair factors to DSBs (3). Despite all the advances in understanding of DDR, how DSBs are initially and precisely recognized is largely unknown.

NAD^+-dependent deacylase sirtuins regulate DDR, DNA repair and genomic integrity. Seven Sirtuins (SIRT1-7) with various enzymatic activities and physiological functions are identified in mammalian cells (4). Particularly, depletion of *Sirt1*, *6* or *7* causes growth retardation, defective DDR and DNA repair and premature aging (5-7). Upon DNA damage, SIRT1 redistributes on chromatin, colocalized with γH2AX, and deacetylates XPA, NBS1 and Ku70, thus regulating nucleotide excision repair (NER), homologous recombination (HR) and non-homologous end-joining (NHEJ) (8-11). Depleting *Sirt1* in mouse fibroblasts impairs DDR and leads to genomic instability (6). SIRT6 is one of the earliest factors recruited to DSBs, which initiates the subsequent recruitment of SNF2H, H2AX, DNA-PKcs and PARP1 (12-15). SIRT6 mono-ribosylates PARP1 and thus to enhance its activity (16). Despite the rapid mobilization to DNA breaks, mechanisms initiating the recruitment of sirtuins are obscure (7,17,18).

Here, we found that SIRT6 polymerizes and directly recognizes DSBs via a putative DNA-binding pocket consisting of N- and C-termini from 2 adjacent molecules. SIRT1 interacts with SIRT6 and deacetylates it at K33, thus allowing its polymerization and recognition of DSBs. K33R mutant, mimicking hypoacetylated SIRT6, rescues DNA repair defects in *SIRT1* KO cells. Our data highlight a synergistic action of Sirtuins in the spatiotemporal regulation of DDR.

Results

SIRT6 directly recognizes DNA double-strand breaks

Upon DNA damage, nuclear SIRTs (SIRT1/6/7) are quickly mobilized to DSBs (Figure S1), serving as a scaffold for DDR and DNA repair (7,17,18). Intriguingly, SIRTs are also activated by RNA and nucleosome (19,20). We reasoned that SIRTs might directly sense DNA breaks, especially DSBs. To test the hypothesis, a molecular docking simulation assay was performed using AutoDock Vina program (21). Crystal structures for SIRT1 (PDB code 4I5I) (22), SIRT6 (3PKI) (23) and SIRT7 (5IQZ) (24) were obtained from Protein Data Bank (https://www.rcsb.org). Heteroatoms were removed and Gasteiger charges were added to atoms. A DSB structure was extracted from PDB code 4DQY (25). As SIRTs use NAD^+ as co-substrate in the amide bond hydrolysis, which shares similar skeleton of phosphate, base and ribose groups to the broken ends of DSB, we included NAD^+ as simulation control. As shown (Figure 1A), the binding affinity between NAD^+ and all nuclear SIRTs are within the range of –8 to –10 kcal/mol. Surprisingly, only the binding between DSB and SIRT6 is energetically favored (–12.7 kcal/mol), even lower than that of NAD^+ (Figures 1A,B). This suggests a direct binding between DSB and SIRT6 and prompted us to gain further experimental evidences. We applied a DSB-mimicking biotin-conjugated DNA duplex and did *in vitro* pulldown assay. Remarkably, recombinant SIRT6 (rSIRT6), but not rSIRT1 or rSIRT7, bounded to the DNA duplex (Figure 1C). This finding was verified by a fluorescence polarization (FP) assay using Fam-labeled DNA duplex. A dynamic fluorescence polarization was observed (Figure 1D, Kd = 166.3 nM), supporting a specific and direct binding of DNA duplex to rSIRT6. By contrast, fluorescence polarization was hardly detected for rSIRT1 or rSIRT7. To interrogate whether such binding is specific to broken DNA, the pulldown assay was again conducted in presence of unlabeled linear or circular DNA. While linearized DNA inhibited the binding of rSIRT6 to DNA duplex, circular one hardly did (Figure 1E). Together, the data indicate the direct recognition of DSB by SIRT6, but not SIRT1 or SIRT7.

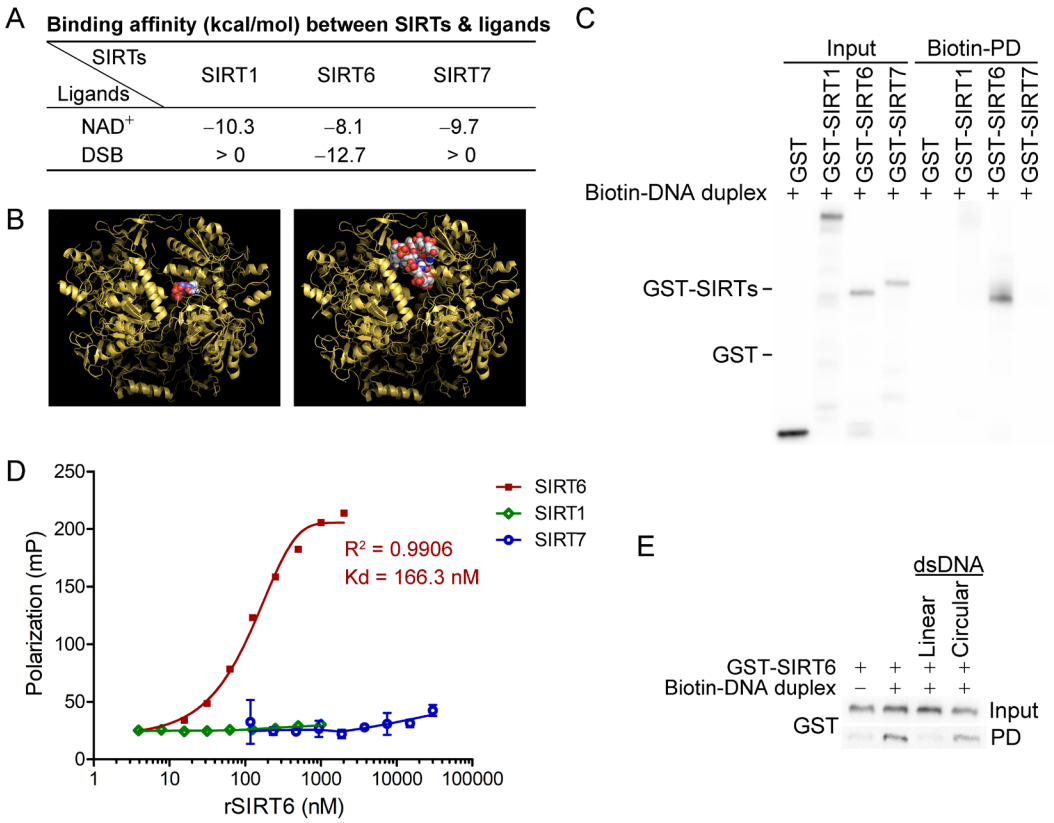

Figure 1. SIRT6 directly recognizes DNA breaks.

(**A**) Predicted binding affinity (kcal/mol) between sirtuins (SIRTs) and ligands.

(**B**) Molecular docking of DSB (right) and NAD^+ (left) with SIRT6.

(**C**) Biotin-labeled DNA duplex were incubated with indicated recombinant SIRTs. Streptavidin beads pulldown was blotted with anti GST and anti SIRT1 antibodies.

(**D**) Fluorescence polarization (FP) of Fam labeled DNA was detected after incubating with GST-SIRT1, GST-SIRT6 or GST-SIRT7.

(**E**) Pulldown assay of Biotin-labeled DNA duplex with GST-SIRT6 in the presence of unlabeled linear DNA or circular DNA.

Dynamic K33 (de)acetylation regulates SIRT6-sensing DSBs

As predicted from the crystallographic data, SIRT6 forms asymmetric hexamer (23), generating three potential DSB binding pockets; each consists of two N-termini and two C-termini from two adjacent molecules (Figure S2A). Both N- and C-termini are essential for the chromatin association of SIRT6 (26). To gain biochemical evidence of SIRT6 polymerization, we employed a biomolecule fluorescence compensation system

(BiFC). *SIRT6* cDNA was cloned to either the N-terminal or C-terminal of a yellow fluorescence protein (YFP), namely N-SIRT6 and C-SIRT6. Yellow fluorescence is detectable by FACS only when N-SIRT6 directly interacts with C-SIRT6. These constructs were co-transfected into HEK293 cells. As shown, a strong fluorescence signal was detected by FACS in more than 24% cells (Figure S2B), suggesting a direct interaction between SIRT6 molecules. Such polymerization of SIRT6 was confirmed by co-immunoprecipitation (Co-IP) in HEK293 cells wherein FLAG-SIRT6 and HA-SIRT6 were co-overexpressed. As shown, FLAG-SIRT6 was detected in the anti HA-SIRT6 immunoprecipitates (Figure S2C).

The phosphate backbone of DSB is negative charged. A positive-charged environment in SIRT6 favors its binding to DSBs. Indeed, one predicted DSB-binding pocket formed by two adjacent molecules in SIRT6 hexamer consists of six positive-charged residues at the edge, i.e. 4 arginines (R32/39) and 2 lysines (K33) (Figure S2D). Acetylation belongs to the most redundant posttranslational modifications, which can turn positive-charged K to neutral Kac. This property is utilized by proteins with lysine-rich domain (KRD), e.g. Histones, Ku70 and p53, for dynamic interaction with proteins harboring acidic domain like SET (27). The heterodimerized Ku70 and Ku80 directly senses DSBs by the flexible C-termini with multiple Ks, and regulates non-homologous end joining (NHEJ) (28). We therefore examined whether SIRT6 is (de)acetylated. FLAG-SIRT6 was immunoprecipitated with anti-FLAG antibody and blotted with anti Kac antibodies. As shown, acetylated Ks was detected in the precipitated FLAG-SIRT6 (Figure 2A). We further purified FLAG-SIRT6 and did high-resolution LC-MS/MS to identify Ks undergoing acetylation. Potential acetylated Ks were summarized (Table S1). In N-terminus, K15 and K33 were identified. To confirm these acetylated Ks, we did point mutagenesis on K15/17/33; K17 was included as control. While neither K15R nor K17R affected the acetylation level of FLAG-SIRT6, K33R significantly inhibited it (Figures 2A and S3), supporting that K33 undergoes dynamic (de)acetylation.

To understand the function of K33 acetylation, we examined whether it is required for the DSB binding of SIRT6. We mutated lysine to arginine (K33R) or glutamine (K33Q) to mimic the deacetylated or acetylated SIRT6 (29). SIRT6 histidine 133 was mutated to tyrosine (H133Y, HY) to blunt SIRT6 enzyme activity (18). The binding of K33Q and H133Y to the DNA duplex was significantly compromised compared to WT and K33R (Figure 2B). Consistently, fluorescence polarization was recorded for SIRT6

K33R (Kd = 104.9 nM), which was hardly detected in case of SIRT6 K33Q (Figure 2C). Of note, H133 is critical for chromatin enrichment of SIRT6 (26). We further monitored GFP-SIRT6 mobility upon DNA damage. GPF-SIRT6 WT, K33Q, K33R and H133Y were reconstituted in *Sirt6*$^{-/-}$ cells and their recruitment to DSBs was monitored. While K33Q and H133Y significantly jeopardized the efficient recruitment to DNA breaks, K33R completely retained such ability (Figures 2D-E). To gain more experimental support, we applied an inducible DR-GFP reporter system, which contains a unique I-*Sce*I cutting site. In presence of triamcinolone acetonide (TA), the I-*Sce*I-GR enzyme translocated to the nucleus within 10 min and generated DSBs, evidenced by increased γH2AX level (Figure 2F-G). The occupancy of SIRT6 on chromatin surrounding DSBs is detected by chromatin immunoprecipitation (ChIP) and quantitative PCR (30). The result showed that both K33Q and H133Y compromised the recruitment of SIRT6 to the sites of damage, whereas K33R remained as efficient as WT (Figures 2H). Of note, K33Q and H133Y also differed the recruitment of SNF2H to DSBs (Figure 2I), which is accomplished by SIRT6 (18). By contrast, SNF2H recruitment was merely altered by K33R. Neither K33R nor K33Q affected the deacetylase activity of SIRT6 (Figure S4).

We next analyzed whether dynamic K33 (de)acetylation modulates the polymerization of SIRT6. HA-SIRT6 and various FLAG-SIRT6 mutants were co-overexpressed and Co-IP was performed. FLAG-SIRT6 was observed in the anti-HA immunoprecipitates, supporting polymerization of SIRT6 (Figure S2C). While HA-SIRT6 bonded to K33R to a similar extent as WT, its binding to K33Q was significantly jeopardized. Of note, H133Y, the enzyme-dead mutation, also jeopardized polymerization of SIRT6. This is indeed consistent with the finding that H133, in addition to the deacetylase activity of SIRT6, is important for its chromatin association (26). The jeopardized polymerization is confirmed by BiFC assay (Figure S5A,B). Together, the data implicate that dynamic K33 (de)acetylation modulates SIRT6 polymerization and thus DSB binding.

Figure 2

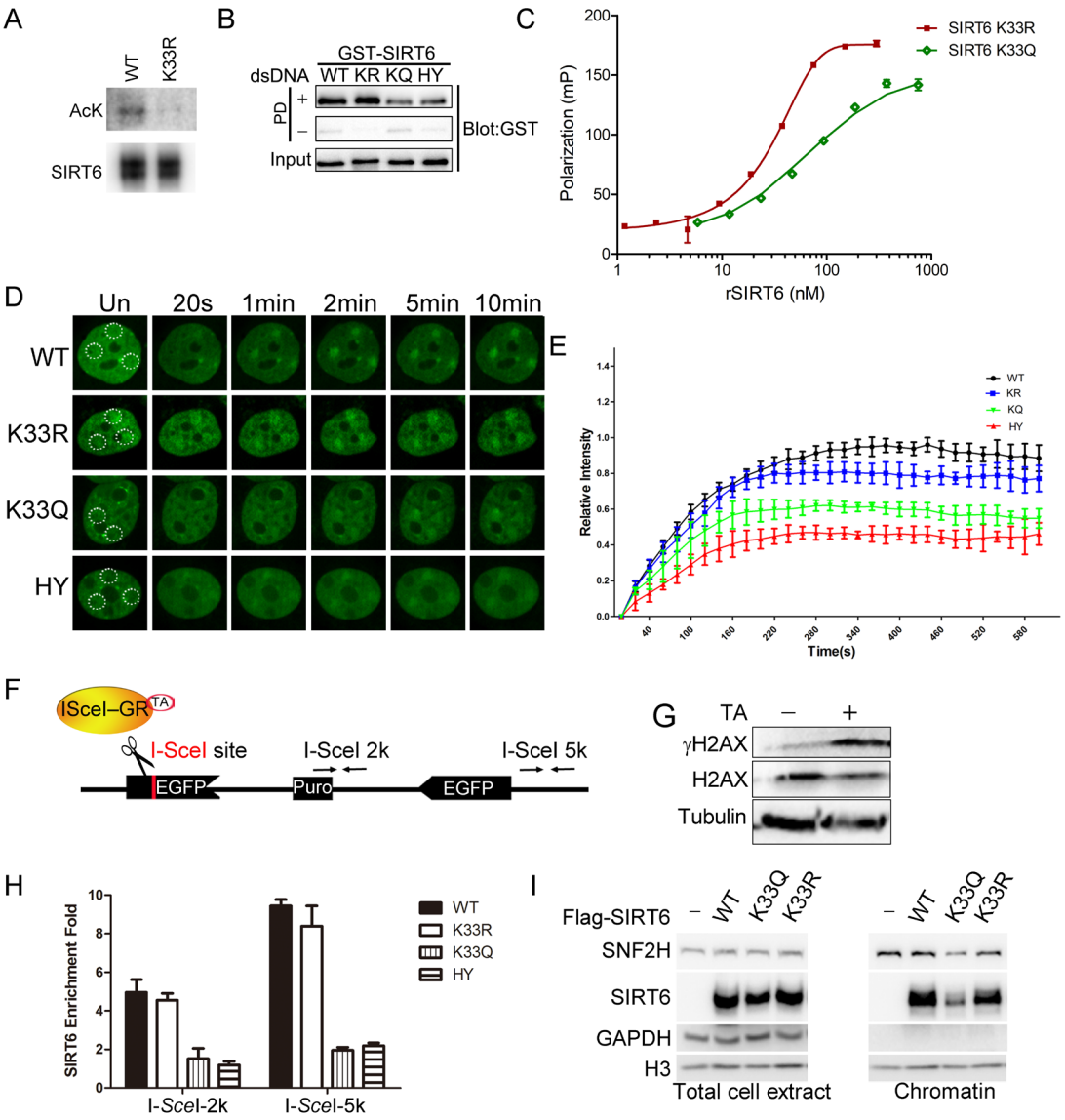

Figure 2. SIRT6 K33 (de)acetylation regulates the DSB binding

(**A**) The acetylation of WT and K33R mutated SIRT6.

(**B**) Pulldown assay of Biotin-labeled DNA duplex with indicated GST-SIRT6.

(**C**) Fluorescence polarization (FP) of Fam labeled DNA was detected after incubating with GST-SIRT6 K133R or K133Q.

(**D-E**) Dynamic recruitment of GFP-SIRT6, K33R, K33Q and HY (H133Y) to the laser-induced DNA breaks. Representative images were shown (**D**) and the white dot circles indicate the damage sites. The relative intensity was calculated by software Fiji (Image J®) (**E**).

(**F**) Schematic map of DR-GFP construct, which contains a single I-*Sce*I site to create

DNA break in the presence of triamcinolone acetonide and I-*Sce*I endonuclease. The amplification primers 2K and 5K downstream I-*Sce*I site used for q-PCR were labeled.
(**G**) Successful generation of DNA breaks in DR-GFP stably transfected Hela cells after triamcinolone acetonide (TA) treatment for 20min, evidenced by elevated γH2AX staining.
(**H**) ChIP-PCR analysis showing the enrichment of SIRT6 and various mutants at the vicinity of DNA breaks. Relative expression of SIRT6 were confirmed by Western blotting. Q-PCR data was normalized to Input DNA and sample without treatment of I-*Sce*I endonuclease (no cut). $*P < 0.05$.
(**I**) Cell fraction analysis showing chromatin enrichment of SNF2H, SIRT6 in FLAG-SIRT6, K33R, K33Q and HY reconstituted *SIRT6* KO HEK293T cells.

SIRT6 is a deacetylation target of SIRT1

We noticed that the level of acetyl SIRT6 was largely elevated in the presence of class III HADC (SIRTs) inhibitor nicotinamide (NAM) or SIRT1-specific inhibitor Ex527, but not class I/II HADC inhibitor Trichostatin A (TSA) (Figure S6). This suggests that SIRT1 is likely involved in SIRT6 deacetylation. Indeed, Co-IP and Western blotting revealed that FLAG-SIRT6 interacted with endogenous SIRT1 (Figure 3A) and FLAG-SIRT1 interacted with endogenous SIRT6 in HEK293 cells (Figure 3B). In addition, SIRT1 was detected in the anti SIRT6 immunoprecipitates and *vice versa* (Figure 3C,D). Determined by GST pulldown assay, His-SIRT1 was pull down by GST-SIRT6 in the test tubes (Figure 3E). Further, co-localization of SIRT6 and SIRT1 was evidenced by confocal microscopy in cells co-transfected with GFP-SIRT6 and DsRed-SIRT1 or co-stained with specific antibodies (Figures 3F and S7A).

SIRTs contain a conserved Sir2 domain and flexible N- and C-termini. To locate exact SIRT6 domains that interact with SIRT1, we did domain mapping by serially mutating the N- and C-terminus as reported (26) (Figure S7B,C). Western blotting analysis showed that the interaction between SIRT6 and SIRT1 was completely abolished in case that N- or C-terminus-deleted SIRT6 was examined (Figure 3G). The data indicate that SIRT6 physically interacts with SIRT1.

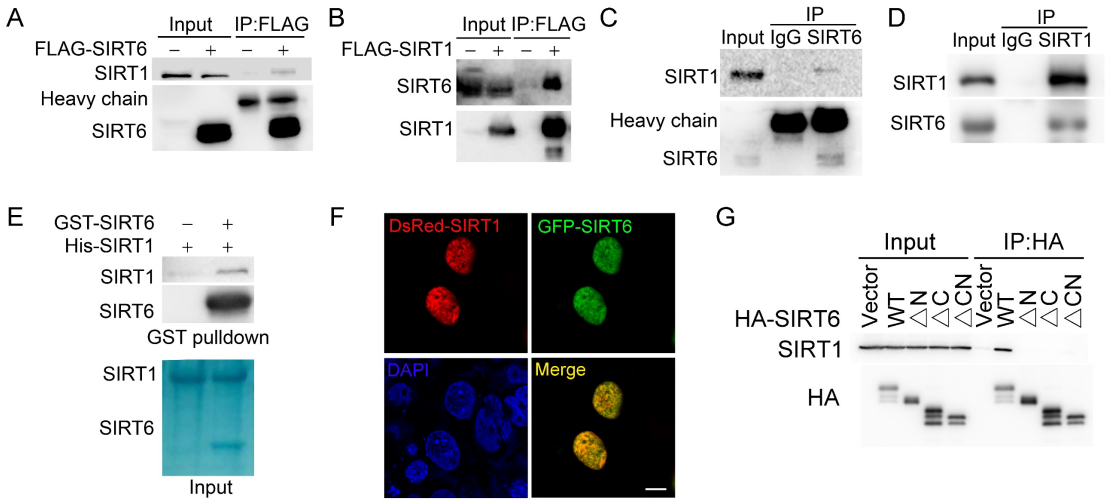

Figure 3. SIRT6 interacts with SIRT1.

(**A**) Western blots showing SIRT1 in anti-FLAG immunoprecipitates in HEK293 cells transfected with FLAG-SIRT6 or empty vector.

(**B**) Western blots showing SIRT6 in anti-FLAG immunoprecipitates in HEK293 cells transfected with FLAG-SIRT1 or empty vector.

(**C**) Western blots showing SIRT1 in anti-SIRT6 immunoprecipitates in Hela cells.

(**D**) Western blots showing SIRT6 in anti-SIRT1 immunoprecipitates in Hela cells.

(**E**) GST pulldown assay showing the interaction between GST-SIRT6 and His-SIRT1 *in vitro*.

(**F**) Representative images showing colocalized DsRed-SIRT1 and GFP-SIRT6 in U2OS cells, determined by confocal microscopy. Scale bar, 10 μm.

(**G**) Co-immunoprecipitation and Western blotting data showing interaction between FLAG-SIRT1 and HA-SIRT6 ΔN (N-terminus deleted), ΔC (C-terminus deleted) and ΔCN (N-/C-termini deleted) in HEK293 cells.

We next examined whether SIRT1 deacetylates SIRT6. As shown, the overexpression of SIRT1 but not other sirtuins inhibited the acetylation of FLAG-SIRT6 (Figure 4A). On the other front, knocking down *SIRT1* significantly upregulated the acetylation level of endogenous SIRT6 in HEK293 cells (Figure 4B). Further, the acetylation level of SIRT6 was decreased in the presence of ectopic SIRT1 rather than its catalytic mutant SIRT1-H366Y (Figure 4C), suggesting SIRT6 likely as a deacetylation target of SIRT1. To test it directly, an *in vitro* deacetylation assay was employed. Recombinant FLAG-

SIRT6 was eluted with FLAG peptide from HEK293 cell lysate. SIRT1 deacetylated SIRT6 in the presence of NAD^+, while NAM inhibited this process (Figure 4D). The deacetylase-inactive SIRT1-HY(S355A) was unable to deacetylate SIRT6. As SIRT1 interacts with the N-terminus of SIRT6, it might deacetylate K33ac. While the acetylation level of SIRT6 was increased in *SIRT1*$^{-/-}$ cells, that of K33R was hardly affected (Figure 4E). Additionally, the acetylation level of SIRT6 K33R was rarely changed upon SIRT1 overexpression (Figure 4F), whereas that of K143/145R was downregulated by ectopic SIRT1 (Figure S8A), supporting K33ac as the main target of SIRT1. By contrast, SIRT1 acetylation level was merely affected when overexpressing SIRT6 in cells (Figure S8B). To further validate the findings, we synthesized a K33ac-containing peptide, and found that it effectively blocked the *in vitro* binding of SIRT6 to SIRT1 (Figure 4G). Of note, GST pulldown assay suggests that the N-terminus rather than the C-terminus of SIRT6 is responsible for its interaction with SIRT1. Together, the data suggest that SIRT1 deacetylates SIRT6 at K33.

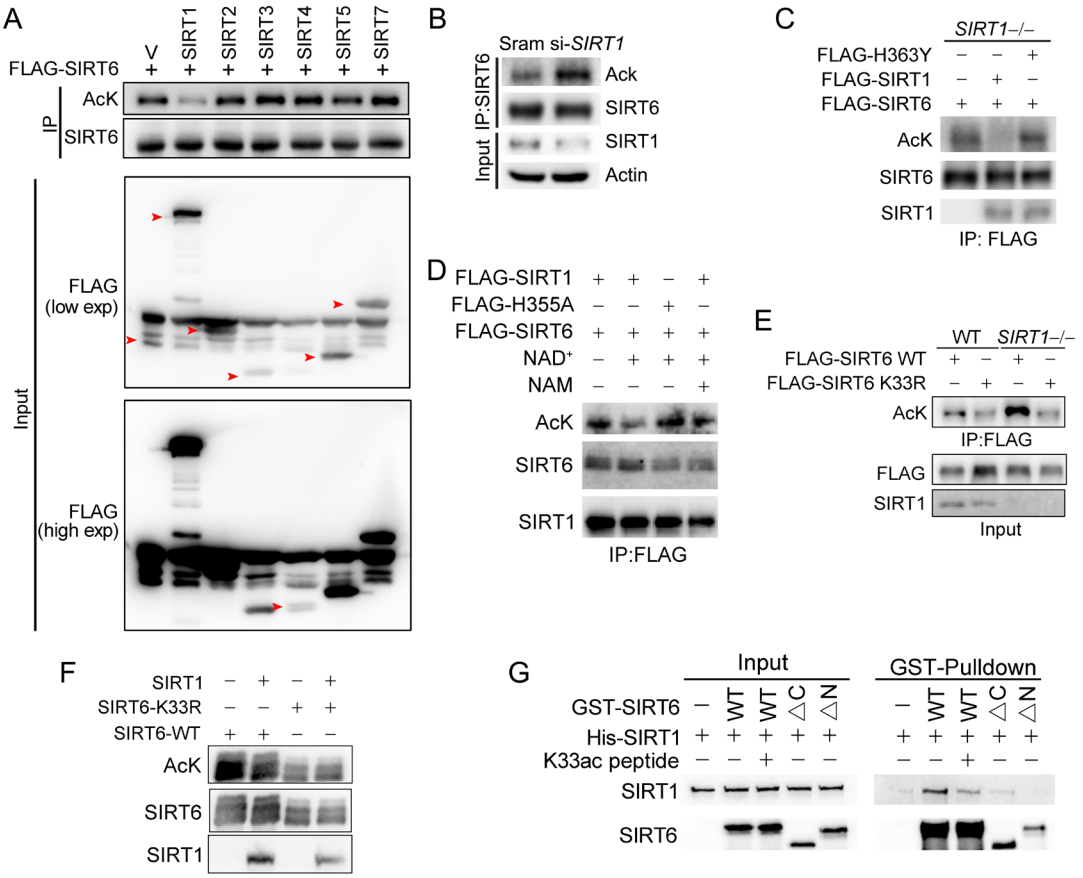

Figure 4. SIRT1 deacetylates SIRT6 at K33

(**A**) The acetylation level of FLAG-SIRT6 in HEK293 cells ectopically expressing SIRT1-5 and SIRT7.

(**B**) The acetylation level of endogenous SIRT6 in HEK293 cells treated si-*SIRT1* or scramble (Sram) siRNAs.

(**C**) The acetylation level of FLAG-SIRT6 in *SIRT1*$^{-/-}$ cells reconstituted with SIRT1 or enzyme-inactive H363Y.

(**D**) The acetylation level of FLAG-SIRT6 in presence of SIRT1, H355A, NAD^+ (500 μM) and/or NAM (2 mM).

(**E**) The acetylation level of FLAG-SIRT6 and K33R in *SIRT1*$^{-/-}$ and WT HEK293 cells.

(**F**) The acetylation level of FLAG-SIRT6 and K33R in HEK293 cells with or without ectopic SIRT1.

(**G**) GST pulldown assay with GST-SIRT6 WT, ΔN, ΔC and His-SIRT1 in presence or absence of 10 μM K33ac peptide (PEELERK(ac)VWELARL), which represents a 14-aa peptide containing acetylated K33 of SIRT6.

γH2AX ensures SIRT6 retention on DSBs

Since the enrichment of SIRT6 at DNA breaks, we asked whether γH2AX was involved in this event. γH2AX is dispensable for the initial DSB recognition but serves as a platform for recruiting DDR factors (2). We thus did Co-IP of endogenous SIRT6 in cells treated with or without CPT. Interestingly, H2AX and γH2AX were detected in anti SIRT6 precipitates only when cells were treated with CPT (Figure 5A,B). Further, *in vitro* pulldown assay with biotin-labeled a C-terminal peptide of γH2AX and H2AX was performed. Consistently, GST-SIRT6 recognized the peptide of γH2AX instead of H2AX (Figure 5C). To study the interacting domain, we purified truncated GST-SIRT6. Peptide pulldown assay revealed that N-terminus truncation was enough to abolish the binding of SIRT6 to γH2AX peptide, while the deletion of C-terminus had little effect (Figure 5D). We then investigated whether SIRT1-mediated deacetylation contributes to the binding of SIRT6 to γH2AX. As shown, K33R mutant efficiently bound to γH2AX in similar extent to WT, but that was abolished in case of K33Q (Figure 5E).

To investigate the functional relevance of SIRT6-γH2AX interaction, we applied laser-induced DNA damage assay and tracked re-location of SIRT6 in MEFs lacking *H2AX*

by immunofluorescence microscopy. As shown, GFP-SIRT6 was immediately recruited to DNA lesions in *H2AX*$^{+/+}$ and *H2AX*$^{-/-}$ MEFs (Figure 5F), implicating that H2AX is dispensable for the initial recruitment of SIRT6. Interestingly, GFP-SIRT6 diminished 10 min after the laser treatment in *H2AX*$^{-/-}$ MEFs but persisted in *H2AX*$^{+/+}$ cells. H2AX is rapidly phosphorylated at serine 139 in response to DSBs (31). When H2AX WT, S139A and S139D were re-introduced into *H2AX*$^{-/-}$ MEFs, the retention of SIRT6 was restored in WT and S139D-re-expressing cells but not S139A (Figure 5G). Together, these data indicate that SIRT6 recognizes γH2AX surrounding DSBs, which is enhanced by SIRT1-mediated deacetylation.

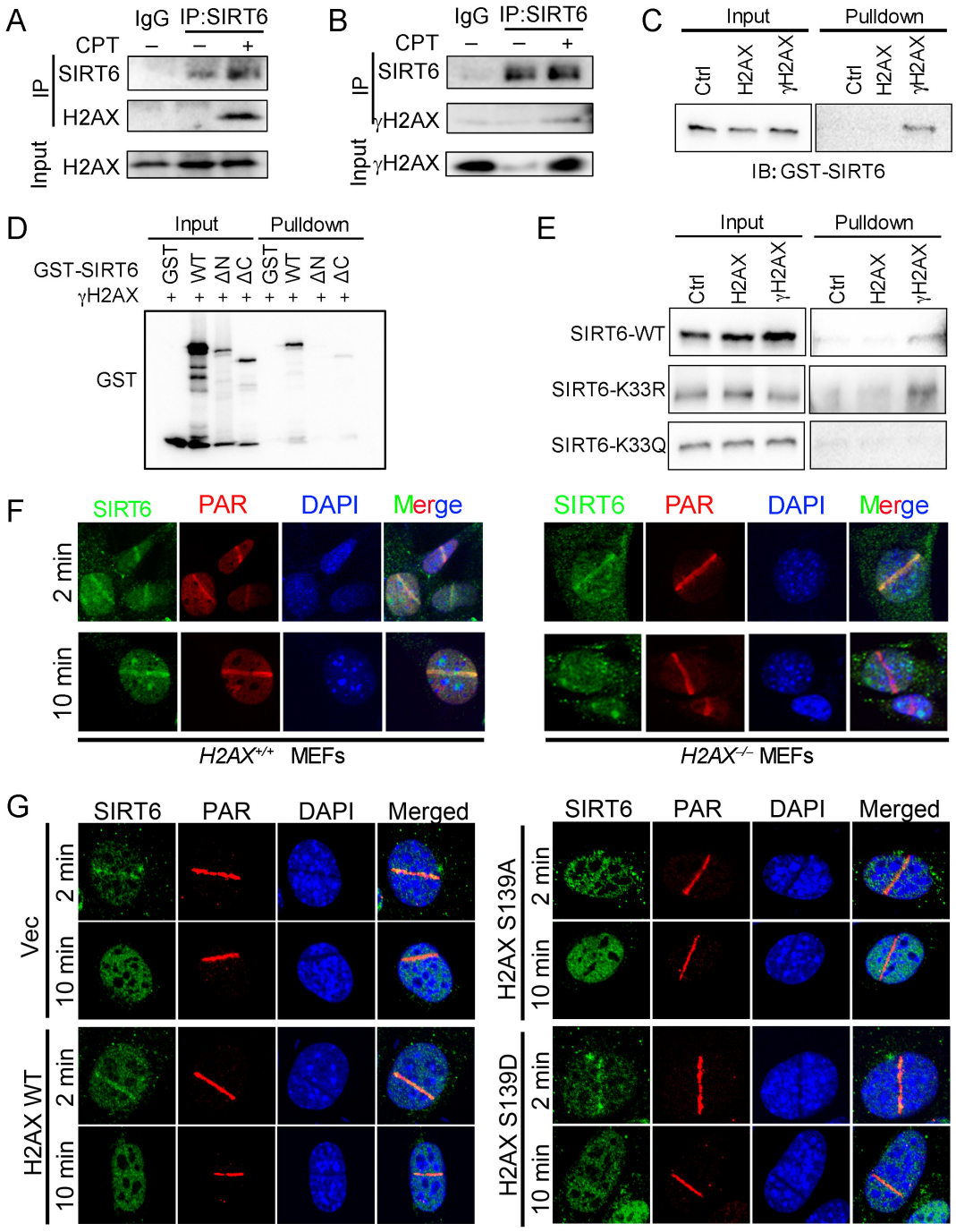

Figure 5. γH2AX is required for the chromatin retention of SIRT6.

(**A**,**B**) Representative immunoblots showing H2AX (A) and γ-H2AX (B) in the anti-SIRT6 immunoprecipitates in HEK293 cells treated with or without camptothecin (CPT).

(**C**) Pulldown assay and Western blotting data showing interaction between GST-SIRT6 and synthesized γH2AX but not H2AX peptide.

(**D**) Pulldown assay and Western blotting showing interaction between synthesized

γH2AX peptide and GST-SIRT6 WT and truncated form (ΔN and ΔC).

(E) Pulldown assay and Western blotting showing interaction between γH2AX peptide and GST-SIRT6 WT, K33R and K33Q.

(**F**,**G**) Laser micropointer analysis of SIRT6 recruitment in *H2AX*$^{+/+}$ and *H2AX*$^{-/-}$ MEFs (**F**), and in *H2AX*$^{-/-}$ MEFs reconstituted with H2AX WT, S139D mimicking hyper-phosphorylation or S139A mimicking hypo-phosphorylation (**G**). PAR immunostaining reveals the damage site. Scale bar, 10 μm.

SIRT1 and SIRT6 cooperatively promote DNA repair

The physical interaction between SIRT1 and SIRT6 prompted us to investigate whether SIRT1 and SIRT6 cooperatively modulate DDR and DNA repair. The DR-GFP reporter system and ChIP-PCR analysis were applied. The recruitment of FLAG-SIRT6 to DSB vicinity was significantly reduced when *SIRT1* was silenced by siRNA (Figures 6A-B). We further analyzed the dynamic recruitment of GFP-SIRT6 upon laser-induced DNA damage. GFP-SIRT6 was rapidly recruited to DNA breaks in WT cells, but this process was largely deferred in *Sirt1*$^{-/-}$ cells (Figures 6E-F), suggesting an indispensable role of SIRT1 in the initial recruitment of SIRT6 to DSBs. By contrast, the recruitment of SIRT1 to DSBs was merely affected by SIRT6 downregulation, as determined by ChIP-PCR analysis and laser micropointer assay (Figures 6C-D,G).

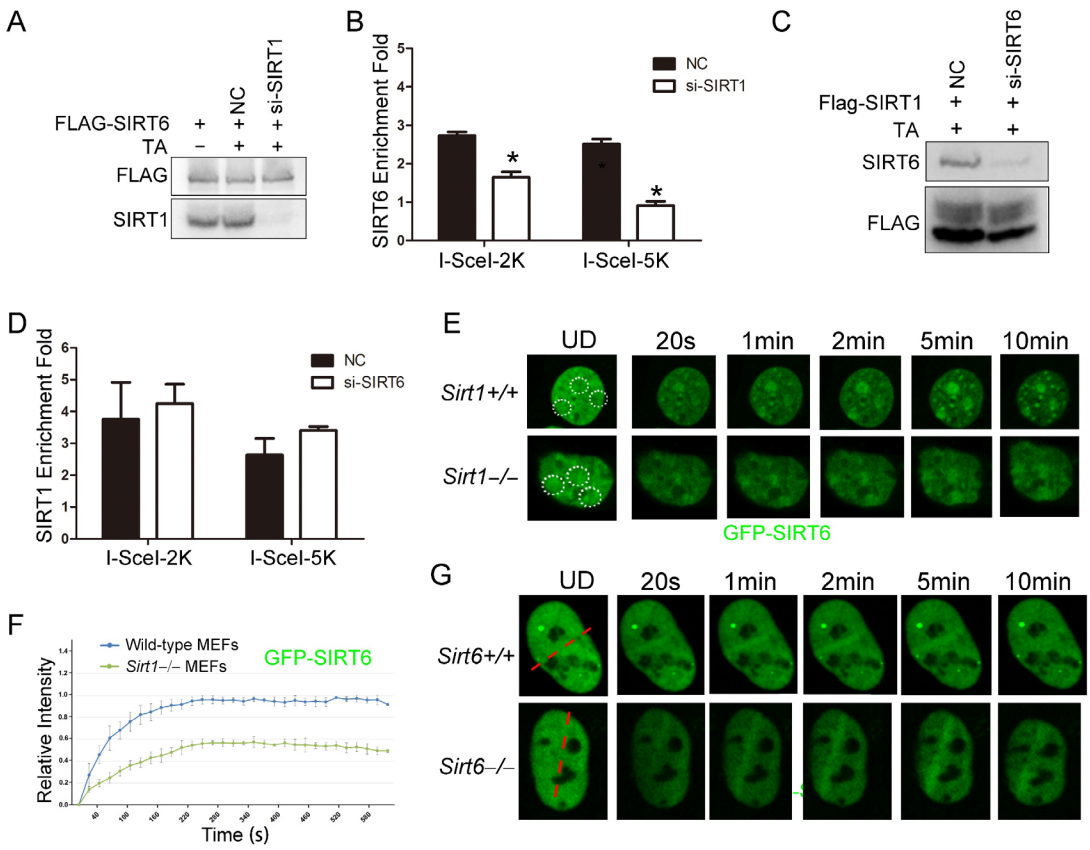

Figure 6. SIRT1 facilitates SIRT6 recruitment in DDR.

(**A**,**B**) ChIP-qPCR analysis showing the enrichment of SIRT6 in DSB vicinity in cells treated with si-*SIRT1* siRNA or scramble (NC). Immunoblots showing protein levels of FLAG-SIRT6 and SIRT1.

(**C**,**D**) ChIP-qPCR analysis showing the enrichment of SIRT1 in DSB vicinity in cells treated with si-*SIRT6* siRNA or NC. Western blots showing protein levels of FLAG-SIRT1 and SIRT6.

(**E**,**F**) GFP-SIRT6 was introduced into and *Sirt1*$^{-/-}$ and *Sirt1*$^{+/+}$ MEFs and fluorescence signal was captured after laser damage at various time points. Representative images were shown (**E**) and relative intensity was calculated by Image J® (**F**). White dot circles indicate the damage sites. Scale bar, 10 μm.

(**G**) GFP-SIRT1 were introduced into and *Sirt6*$^{-/-}$ and *Sirt6*$^{+/+}$ MEFs and fluorescence signal was captured after laser damage at various time points. Representative images were shown. Scale bar, 10 μm

We next assessed the function of SIRT6 deacetylation in DNA repair. We found that the

acetylation level of SIRT6 was significantly decreased upon CPT treatment, which was abolished in case of SIRT6 K33R or lack of *SIRT1* (Figure 7A), implying that SIRT6 is deacetylated by SIRT1 upon DNA damages. We examined the effect of SIRT6 mutants on DNA repair by comet assay, which assesses repair ability at single cell level. To this end, K33R and K33Q were overexpressed in *SIRT6*$^{-/-}$ cells and DNA repair efficacy was examined. As shown, overexpression of SIRT6 significantly enhanced the DNA repair efficacy upon CPT treatment, while K33Q or H133Y lost the ability. By contrast, K33R promoted DNA repair to an extent comparable to WT (Figure 7B). Together, the data implicate that deacetylation of SIRT6 at K33 is indispensable for DNA repair.

SIRT1 regulates DNA repair (6). To elucidate the synergistic effects of SIRTs in DNA repair, we examined whether hyper-acetylation of SIRT6 underlines the defective DNA repair in *SIRT1*$^{-/-}$ cells. As shown, SIRT6, K33R and SIRT1 rescued the defective DNA repair imposed by *SIRT1* deficiency, while SIRT6 K33Q and H133Y merely did (Figure 7C). Similar phenomena were observed in Hela cells (Figure S8B-C). HR assay showed that SIRT6 WT and K33R enhanced HR capacity, whereas neither K33Q nor H133Y did (Figure 7D). Further, compared to WT and K33R, K33Q significantly inhibited the colorization of transfected Hela cells (Figure 7E). SIRT6 WT and K33R enhanced cell survival after ionized radiation (Figure 7F).

Altogether, the above data implicate a synergistic action between SIRT1 and SIRT6 in regulating DDR and DNA repair. We propose a model–SIRT6 is deacetylated by SIRT1 at K33, thus promoting its polymerization and recognition of DSBs; K33-deacetylated SIRT6 anchors to γH2AX, allowing expansion and retention on the chromatin flanking DSBs and subsequent remodeling, likely via deacetylating H3K9ac (Figure 7G).

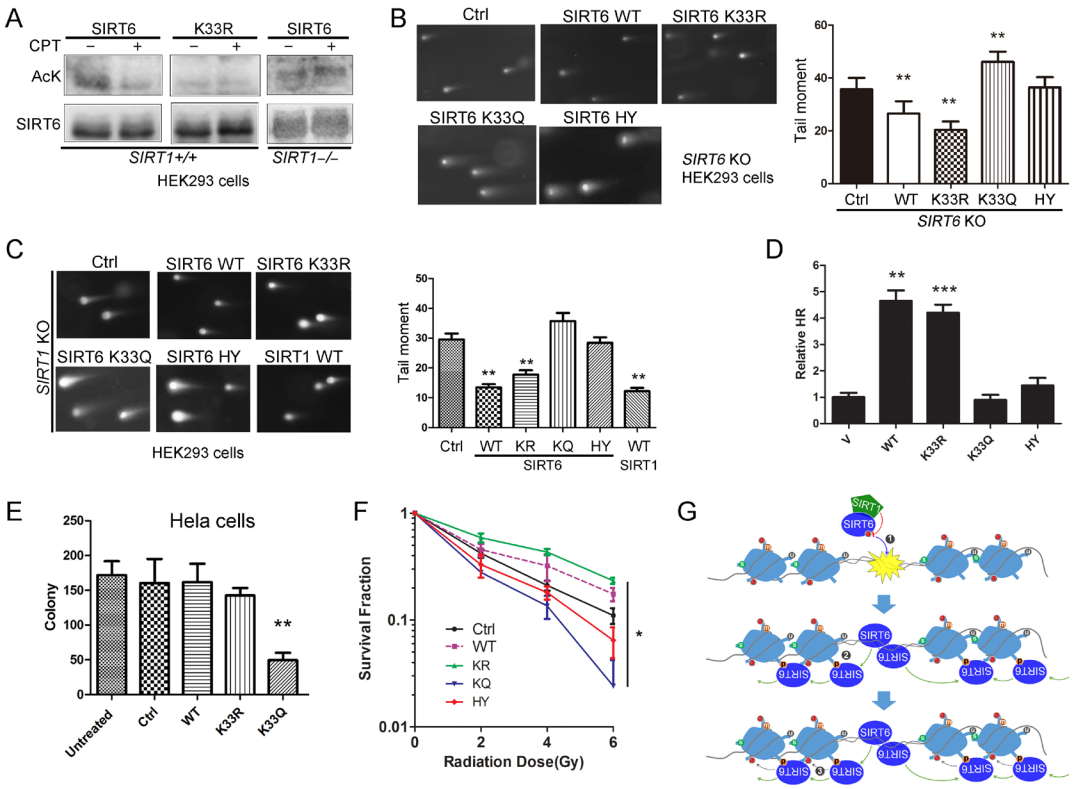

Figure 7. SIRT6 rescues DNA repair defects caused by SIRT1 deficiency.

(**A**) The acetylation level of SIRT6 and K33R in *SIRT1*$^{+/+}$ and *SIRT1*$^{-/-}$ HEK293 cells treated or untreated with CPT (1 μM) for 1 h.

(**B**) Comet assay in FLAG-SIRT6, K33R, K33Q and HY reconstituted *SIRT6* KO cells treated with CPT for 1 h. Data are represented as mean ± s.e.m. $^{**}P < 0.01$.

(**C**) Comet assay in *Sirt1*$^{-/-}$ cells transfected with FLAG-SIRT6, K33R, K33Q, HY and SIRT1 and treated with CPT for 1 h. Data are represented as mean ± s.e.m. $^{**}P < 0.01$.

(**D**) HR assay in U2OS cells ectopically expressing FLAG-SIRT6, K33R , K33Q or HY. The relative HR value was normalized with vector control. Data are represented as mean ± s.e.m. ***P < 0.001. **P < 0.01.

(**E**) Colony-forming assay in Hela cells ectopically expressing FLAG-SIRT6, K33R or K33Q. Data are represented as mean ± s.e.m. $^{**}P < 0.01$.

(**F**) Colony-forming assay in Hella cells stable expressing SIRT6 WT, K33R, K33Q or HY after radiation at indicated dose. Data are represented as mean ± s.e.m. *P < 0.05.

(**G**) A working model: (a) SIRT6 is deacetylated by SIRT1 at K33, which promotes SIRT6 polymerization and recognition of DSBs. (b) Beyond DSBs, K33-deacetylated SIRT6 anchors to γH2AX and expands on local chromatin flanking DSBs. (c) SIRT6 mediates local chromatin remodeling via deacetylating H3K9ac.

Discussion

DDR is highly orchestrated and initiated by DNA break-sensing (1). The MRN complex (32), Ku complex (28), RPA (33) and PARP1 (34,35) directly recognize DSBs. SIRTs are among the earliest factors that are recruited to DSBs (17,18), facilitating recruitment of PARP1 (7). Consistent with published data (23), we found that SIRT6 oligomerizes and recognizes DSBs via a DSB-binding pocket generated by the N- and a C-termini of two adjacent molecules. This is consistent with a report showing that both N- and C-termini are essential for chromatin association of SIRT6 (26). Recently, using a super-resolution fluorescent particle tracking method, Yang et al found that the binding of PARP1 to DSBs happens earlier than SIRT6 but transient (36). One possible explanation is that, PARP1 is first recruited to DSBs; later-on recruited SIRTs directly by DSBs facilitates the stabilization and expansion of PARP1 in surrounding region.

SIRTs share similar functions in DDR and DNA repair; upon DNA damage, both SIRT1 and SIRT6 are rapidly mobilized to DSBs (7,17,18). SIRT1 redistributes on chromatin and deacetylates XPA, NBS1 and Ku70 to promote DNA repair (8-11). SIRT6 mono-ribosylates PARP1 to enhance its activity (16), and facilitates subsequent recruitment of SNF2H, H2AX and DNA-PKcs (12-15). Here we revealed a synergistic action between nuclear SIRTs – SIRT1 deacetylates SIRT6 to promote its mobilization to DSBs. K33R mutant, mimicking hypo-acetylated SIRT6, rescues DNA repair defects in *SIRT1* null cells. Interestingly, phosphorylation of SIRT6 on S10 by JNK promotes subsequent recruitment itself and PARP1 upon oxidative stress, also supporting an essential role of N terminus for DSB-recruitment (15). Consistent with the cooperative action between SIRT1 and SIRT6, independent studies revealed interaction between SIRT1 and SIRT7, showing that SIRT1 recruits SIRT7 to promote cancer cell metastasis (37), and that SIRT1 and SIRT7 antagonistically regulate adipogenesis (38).

The acetylation levels of H3K9 and H3K56 decrease upon DNA damage and then goes back to original level (39). SIRT1 and SIRT6 are the deacetylases of H3K9ac and H3K56ac; both are recruited to DSBs upon DNA damage, indicating that SIRT1 and/or SIRT6 might contribute to the reduced H3K9ac and H3K56ac level. In addition, although mechanistically unclear, the levels of H3K9ac and H3K56ac are negatively correlated with γH2AX. In current study, we found γH2AX is not required for recruiting

SIRT6 at the beginning but indispensable for the retention of SIRT6 on local chromatin surrounding DSBs. This is consistent with reports that γH2AX is dispensable for initial reorganization of DNA breaks but rather serves as a platform to stabilize repair factors like NBS1, 53BP1 and BRCA1 (2). SIRT6 might deacetylate H3K9ac and/or H3K56ac surrounding DSBs, bridging γH2AX to chromatin remodeling. Together, the findings provide a scenario how γH2AX and histone modifiers coordinate to amplify DDR.

SIRT6 together with SNF2H stabilize γH2AX foci (40). Here we found that γH2AX is required to anchor SIRT6 to DSBs, providing a positive feedback regulation between SIRT6 and γH2AX. It is consistent with reports showing a distinct reduction of γH2AX and improper DDR in *Sirt6*$^{-/-}$ and *Sirt1*$^{-/-}$ cells. Recent advances suggest electrostatic force between negative charge phosphate group and positive charge lysine as a novel form of protein-protein interaction (27). It is plausible to speculate that (de)acetylation might act as a switch to modulate such interaction between SIRT6 and γH2AX.

Known as longevity-associated genes, SIRT6 and SIRT1 are redundant in DNA repair but not replaceable. In this study, we identified a direct binding of SIRT6 to DNA breaks, and physical and functional interaction between SIRT6 and SIRT1. SIRT6 rescues DNA repair defects imposed by SIRT1 deficiency. Overall, these data highlight a synergistic action of nuclear SIRTs in the spatiotemporal regulation of DDR and DNA repair.

Materials and Methods

Antibodies, Oligos and Plasmids

Commercial antibodies used in this study includes: SIRT6, SNF2H, pan-AcK, H3 and γH2AX (Abcam), H2AX, SIRT1 and GST (CST), H3K9ac and H3K56ac (Millipore), SIRT6 (Novus), Tubulin and FLAG (Sigma).

Oligos used for RNA interference:
siSIRT6, 5'-AAGAAUGUGCCAAGUGUAAGA-3';
siSIRT1, 5'-ACUUUGCUGUAACCCUGUA-3'.
Primers used for ChIP qPCR:
I-SceI- 2k-F, 5'-GCCCATATATGGAGTTCCGC-3';
I-SceI-2k-R, 5'-GGGCCATTTACCGTCATTG-3';
I-SceI-5k-F, 5'-GTTGCCGGGAAGCTAGAGTAAGTA-3';

I-SceI-5k-R, 5'-TTGGGAACCGGAGCTGAATGAA-3'.

gRNA used for CRISPR/Cas9 gene editing:

Hu Sirt6: gRNA-F, 5'-CACCGGCTGTCGCCGTACGCGGACA-3';

gRNA-R, 5'-AAACTGTCCGCGTACGGCGACAGCC-3'.

Hu Sirt1: gRNA-F, 5'-CACCGATAGCAAGCGGTTCATCAGC-3'

Human SIRT6 was cloned into pCDNA3.1 with FLAG; 3×FLAG-SIRT1 was ordered from Addgene. SIRT6ΔC and ΔN were amplified with specific primers and cloned into pKH3HA and pGex vector. KR, KQ and HY mutants were obtained by converting SIRT6 lysine 33 to arginine (KR), or to glutamine (KQ) and SIRT6 133 histidine to tyrosine (HY) via directed mutagenesis described below in detail.

Site-directed mutagenesis

The primers used for mutagenesis were designed using the online Quick Change Primer Design Program provided by Agilent Technologies. The mutagenesis was performed using Pfu DNA polymerase (Agilent) and 300 ng plasmid template according to the manufactory's instruction. The PCR product was digested by DpnI endonuclease for 1h at 37°C, followed by transformation and sequencing.

Primer used for generation of SIRT6 KR, KQ and HY mutants:

KR forward: 5'-GGAGCTGGAGCGGAGGGTGTGGGAACT-3'
KR reverse: 5'-AGTTCCCACACCCTCCGCTCCAGCTCC-3'

KQ forward: 5'-GGAGCTGGAGCGGCAGGTGTGGGAACT-3'
KQ reverse: 5'-AGTTCCCACACCTGCCGCTCCAGCTCC-3'

HY forward: 5'-ACAAACTGGCAGAGCTCTACGGGAACATGTTTGTG-3'
HY reverse: 5'-CACAAACATGTTCCCGTAGAGCTCTGCCAGTTTGT-3'

Immunoprecipitation

HEK293T cells were transfected with indicated plasmids using Lipofetamine®3000 (Invitrogen, USA), according to the manufacturer's instructions. Cells were lysed 48 h post-transfection in lysis buffer (50 mM Tris-HCl, pH 7.4, 200 mM NaCl, 0.2% NP40, 10% glycerol, 1mM NaF, 1 mM Sodium butyrate, 10 mM Nicotinamide and complete protease inhibitor cocktail, Roche). The cell extracts were incubated with anti-FLAG M2 monoclonal antibody-conjugated agarose beads (Sigma) at 4℃ overnight. The

immunoprecipitates were boiled with 2×laemmli buffer and were analyzed by Western blotting.

Chromatin Immunoprecipitation (ChIP)

I-*Sce*I-GR assays were performed as described (30). Hela cells stable transfected with DR-GFP were transiently transfected with RFP-I-*Sce*I-GR together with FLAG-SIRT6, KR, KQ or HY. 48 h after transfection, the cells were treated with 10^{-7} M of triamcinolone acetonide (TA, Sangon, Shanghai) for 20 min, and fixed to crosslink chromatin with 1% paraformaldehyde at 37°C for 10 min and stopped with 0.125 M glycine. The chromatin was sonicated to 200bps~600bps and incubated with indicated antibodies. After de-cross linking, ChIP-associated DNA were extracted and examined by quantitative real-time PCR.

Comet assay

Comet assay was performed as described (41). Briefly, after CPT treatment, cells were digested into single cell suspension, mixed with 1% agarose at the density of 1×10^5, coated on the slide and followed by incubating in lysis buffer (2% sarkosyl, 0.5M Na_2EDTA, 0.5 mg/ml proteinase K) overnight. Slides were incubated with N2 buffer (90 mM Tris, 90 mM boric acid and 2 mM Na_2EDTA) and transferred to electrophoresis for 25 min at 0.6 V/cm. Slides were incubated in staining solution containing 2.5 μg/ml of Propidium iodide for 30 min. Images were captured under fluorescent microscope.

Cell fractionation

Cells were scraped and washed with cold PBS. The pellet was resuspended in nuclei lysis buffer (10 mM HEPES, 10 mM KCl, 1.5 mM $MgCl_2$, 0.34M sucrose, 10% glycerol, 1mM DTT, 0.1% TrionX-100.) for 10min on ice and centrifuged at the speed 1300 g for 10 min. The pellet was resuspended in lysis buffer (3 mM EDTA, 0.2 mM EGTA, 1 mM DTT) for 10 min on ice and centrifuged at the speed 1700 g for 10min. The pellet was saved as chromatin fraction.

Micro-point laser irradiation and microscopy

U2OS or MEF cells were seeded on a dish with thin glass bottom (NEST), then locally irradiated with a 365 nm pulsed UV laser (16 Hz pulse, 56% laser output), generated by the micro-point laser illumination and ablation system (Andor®, power supply TPES24-T120MM, Laser NL100, 24V 50W), which is coupled to the fluorescence path

of the Nikon A1 confocal imaging system (TuCam). Fluorescent protein recruitment and retention were continuously monitored with time-lapse imaging every 20 s for 10 min. Quantification of fluorescence intensity at every time-point was measured by Fiji (image J) software.

CRISPR/Cas9-mediated gene editing

CRISPR/Cas9-mediated gene editing was conducted as described (Ran et al.,2013). Briefly, pX459 vector (Addgene#48139) was digested with BbsI and ligated with annealed oligonucleotides. The constructs containing target gRNAs were transfected into HEK293T cells with Lipofetamine3000® (Invitrogen). Cells were selected for 5 days with puromycin 24 h after transfection. Single clone was picked for sequencing.

Peptide pulldown

The C terminus of H2AX (BGKKATQASQEY) and γH2AX (BGKKATQApSQEY) were synthesized and conjugated with biotin (GL Biochem, Shanghai). For one reaction, 1 μg biotinylated peptides were incubated with 1 μg GST-SIRT6 in binding buffer (50 mM Tirs-HCl, 200 mM NaCl, 0.05% NP40) overnight at 4°C. Streptavidin Sepharose beads (GE) was then used to pulldown peptide and protein complexes for 1 h at 4°C, followed by Western blotting.

Immunofluorescence staining

Cells were washed with PBS and fixed with 4% formaldehyde for 20 min, followed by permeabilization with cold methanol (-20°C) for 5 min, blocking with 5% BSA for 30 min, incubation with primary antibodies (SIRT1, 1:200 dilution in 1% BSA; γH2AX, 1:500 dilution in 1% BSA; SIRT6, 1:200 dilution in 1% BSA) for 1 h and secondary antibodies (donkey anti-rabbit IgG Alexa Fluor 594 and donkey anti-mouse IgG FITC from Invitrogen, 1:500 dilution in1% BSA) for 1h at room temperature. Cells were then co-stained with DAPI (Invitrogen) and observed under a fluorescent microscope.

HR assay

U2OS cells stabled transfected with DR-GFP were transfected with HA-I-SceI together with Flag-SIRT6 WT, K33R, K33Q or HY respectively. After transfection for 48h, cells were harvested and analyzed the GFP positive cell ratio per 10^4 cells by flow cytometry (BD). Relative HR efficiency was normalized with vector control.

Colony formation assay

Hella cells were seeded into six-well plates 24 hours after transfection in defined numbers. 24 hours following re-plating the cells were dosed with increased amounts of radiation. Fresh media was added after seven days. Once reached 50 cells in size (10-14 days), colonies were fixed with 20% methanol， and stained with crystal violet. Colonies (>50 cells) were used for analysis. Ionizing radiation was delivered by an X-Rad 320 irradiator (Precision X-Ray Inc. N. Branford, CT , USA).

DNA pulldown assay

DNA binding assay was performed following previous report (42). Briefly, biotin conjugated DNA duplex with the size of 220bp was generated by PCR amplification using biotin-labeled primers and I-sceI plasmid as template. In regard of DNA pulldown assay, 10pmol biotinylated DNA duplex were incublated with 0.5μg indicated recombinant proteins in 300 μl binding buffer (10 mM Tris-Cl pH7.5, 100 mM NaCl, 0.01% NP40 and 10% glycerol) overnight at 4°C. Streptavidin Sepharose beads (GE) were added the next day, and incubated for another 1 hour. The beads were then collected and washed with binding buffer for 3 times. The beads were subsequently boiled in 2×laemmli buffer and analyzed by Western blot. For linear and circular DNA competition assay, the ratios of non-biotin labeled linear/circular DNA to biotin DNA duplex were 5:1 or 10:1. Linear DNA were generated with PCR amplification using non-biotin-labeled primers, and circular DNA were obtained by cloning PCR product into pCDNA 3.1 plasmid.

The sequences used for PCR:

Forward, 5'-TACGGCAAGCTGACCCTGAA-3'
Reverse, 5'-CGTCCTCCTTGAAGTCGATG-bio-3'

Fluorescence polarization assay

SIRT1, SIRT6 and SIRT7 recombinant proteins were purified *in vitro*, and incubated with FAM conjugated DNA duplex (20 nM) for 30 min on ice at indicated concentration. The FP value of each sample was measured on 96 plates using a Multimode Plate Reader VictorTM X5 (PerkinElmer, USA) with excitation wavelength 480 nm and emission wavelength 535 nm. Curve fitting was performed by GraphPad® prism.

Acknowledgements

We thank Dr Linyu Lu (Zhejiang University, China) for providing *H2AX*$^{-/-}$ MEFs. This project was supported by research grants from the National Key R&D Program of China (2017YFA0503900), the National Natural Science Foundation of China (91849208, 81972602, 81702909, 81871114, 81601215), the National Natural Science Foundation of Guangdong Province (2015A030308007, 2017B030301016), Shenzhen Science and Technology Innovation Commission (ZDSYS20190902093401689, KQJSCX20180328093403969, JCYJ20180507182044945), the Youth Foundation of Tianjin Medical University Cancer Institute and Hospital (NO. B1714), and Tianjin Municipal Science Foundation for Youths (NO. 18JCQNJC79800).

Competing interests

The authors declare no competing interests.

REFERENCES

1. Ciccia, A. and Elledge, S.J. (2010) The DNA damage response: making it safe to play with knives. *Mol Cell*, **40**, 179-204.
2. Celeste, A., Fernandez-Capetillo, O., Kruhlak, M.J., Pilch, D.R., Staudt, D.W., Lee, A., Bonner, R.F., Bonner, W.M. and Nussenzweig, A. (2003) Histone H2AX phosphorylation is dispensable for the initial recognition of DNA breaks. *Nature cell biology*, **5**, 675-679.
3. Price, B.D. and D'Andrea, A.D. (2013) Chromatin remodeling at DNA double-strand breaks. *Cell*, **152**, 1344-1354.
4. Houtkooper, R.H., Pirinen, E. and Auwerx, J. (2012) Sirtuins as regulators of metabolism and healthspan. *Nature reviews Molecular cell biology*, **13**, 225-238.
5. Mostoslavsky, R., Chua, K.F., Lombard, D.B., Pang, W.W., Fischer, M.R., Gellon, L., Liu, P., Mostoslavsky, G., Franco, S. and Murphy, M.M. (2006) Genomic instability and aging-like phenotype in the absence of mammalian SIRT6. *Cell*, **124**, 315-329.
6. Wang, R.-H., Sengupta, K., Li, C., Kim, H.-S., Cao, L., Xiao, C., Kim, S., Xu, X., Zheng, Y. and Chilton, B. (2008) Impaired DNA damage response, genome instability, and tumorigenesis in SIRT1 mutant mice. *Cancer cell*, **14**, 312-323.
7. Vazquez, B.N., Thackray, J.K., Simonet, N.G., Kane‐Goldsmith, N., Martinez‐Redondo, P., Nguyen, T., Bunting, S., Vaquero, A., Tischfield, J.A. and Serrano, L. (2016) SIRT7 promotes genome integrity and modulates non‐homologous end joining DNA repair. *The EMBO journal*, e201593499.
8. Fang, E.F., Kassahun, H., Croteau, D.L., Scheibye-Knudsen, M., Marosi, K., Lu, H., Shamanna, R.A., Kalyanasundaram, S., Bollineni, R.C., Wilson, M.A. *et al.* (2016) NAD+ Replenishment Improves Lifespan and Healthspan in Ataxia Telangiectasia Models via Mitophagy and DNA Repair. *Cell metabolism*, **24**, 566-581.
9. Yuan, Z., Zhang, X., Sengupta, N., Lane, W.S. and Seto, E. (2007) SIRT1 regulates the

function of the Nijmegen breakage syndrome protein. *Molecular cell*, **27**, 149-162.

10. Fan, W. and Luo, J. (2010) SIRT1 regulates UV-induced DNA repair through deacetylating XPA. *Molecular cell*, **39**, 247-258.
11. Jeong, J., Juhn, K., Lee, H., Kim, S.H., Min, B.H., Lee, K.M., Cho, M.H., Park, G.H. and Lee, K.H. (2007) SIRT1 promotes DNA repair activity and deacetylation of Ku70. *Exp Mol Med*, **39**, 8-13.
12. Van Meter, M., Simon, M., Tombline, G., May, A., Morello, Timothy D., Hubbard, Basil P., Bredbenner, K., Park, R., Sinclair, David A., Bohr, Vilhelm A. *et al.* (2016) JNK Phosphorylates SIRT6 to Stimulate DNA Double-Strand Break Repair in Response to Oxidative Stress by Recruiting PARP1 to DNA Breaks. *Cell Reports*, **16**, 2641-2650.
13. Atsumi, Y., Minakawa, Y., Ono, M., Dobashi, S., Shinohe, K., Shinohara, A., Takeda, S., Takagi, M., Takamatsu, N., Nakagama, H. *et al.* (2015) ATM and SIRT6/SNF2H Mediate Transient H2AX Stabilization When DSBs Form by Blocking HUWE1 to Allow Efficient γH2AX Foci Formation. *Cell Reports*, **13**, 2728-2740.
14. McCord, R.A., Michishita, E., Hong, T., Berber, E., Boxer, L.D., Kusumoto, R., Guan, S., Shi, X., Gozani, O., Burlingame, A.L. *et al.* (2009) SIRT6 stabilizes DNA-dependent protein kinase at chromatin for DNA double-strand break repair. *Aging (Albany NY)*, **1**, 109-121.
15. Van Meter, M., Simon, M., Tombline, G., May, A., Morello, T.D., Hubbard, B.P., Bredbenner, K., Park, R., Sinclair, D.A. and Bohr, V.A. (2016) JNK Phosphorylates SIRT6 to Stimulate DNA Double-Strand Break Repair in Response to Oxidative Stress by Recruiting PARP1 to DNA Breaks. *Cell Reports*, **16**, 2641-2650.
16. Mao, Z., Hine, C., Tian, X., Van Meter, M., Au, M., Vaidya, A., Seluanov, A. and Gorbunova, V. (2011) SIRT6 promotes DNA repair under stress by activating PARP1. *Science*, **332**, 1443-1446.
17. Dobbin, M.M., Madabhushi, R., Pan, L., Chen, Y., Kim, D., Gao, J., Ahanonu, B., Pao, P.-C., Qiu, Y. and Zhao, Y. (2013) SIRT1 collaborates with ATM and HDAC1 to maintain genomic stability in neurons. *Nature neuroscience*, **16**, 1008-1015.
18. Toiber, D., Erdel, F., Bouazoune, K., Silberman, D.M., Zhong, L., Mulligan, P., Sebastian, C., Cosentino, C., Martinez-Pastor, B. and Giacosa, S. (2013) SIRT6 recruits SNF2H to DNA break sites, preventing genomic instability through chromatin remodeling. *Molecular cell*, **51**, 454-468.
19. Gil, R., Barth, S., Kanfi, Y. and Cohen, H.Y. (2013) SIRT6 exhibits nucleosome-dependent deacetylase activity. *Nucleic Acids Res*, **41**, 8537-8545.
20. Tong, Z., Wang, M., Wang, Y., Kim, D.D., Grenier, J.K., Cao, J., Sadhukhan, S., Hao, Q. and Lin, H. (2017) SIRT7 Is an RNA-Activated Protein Lysine Deacylase. *ACS Chem Biol*, **12**, 300-310.
21. Trott, O. and Olson, A.J. (2010) AutoDock Vina: improving the speed and accuracy of docking with a new scoring function, efficient optimization, and multithreading. *J Comput Chem*, **31**, 455-461.
22. Zhao, X., Allison, D., Condon, B., Zhang, F., Gheyi, T., Zhang, A., Ashok, S., Russell, M., MacEwan, I., Qian, Y. *et al.* (2013) The 2.5 A crystal structure of the SIRT1 catalytic domain bound to nicotinamide adenine dinucleotide (NAD+) and an indole

(EX527 analogue) reveals a novel mechanism of histone deacetylase inhibition. *J Med Chem*, **56**, 963-969.

23. Pan, P.W., Feldman, J.L., Devries, M.K., Dong, A., Edwards, A.M. and Denu, J.M. (2011) Structure and biochemical functions of SIRT6. *J Biol Chem*, **286**, 14575-14587.
24. Priyanka, A., Solanki, V., Parkesh, R. and Thakur, K.G. (2016) Crystal structure of the N-terminal domain of human SIRT7 reveals a three-helical domain architecture. *Proteins*, **84**, 1558-1563.
25. Langelier, M.F., Planck, J.L., Roy, S. and Pascal, J.M. (2012) Structural basis for DNA damage-dependent poly(ADP-ribosyl)ation by human PARP-1. *Science*, **336**, 728-732.
26. Tennen, R.I., Berber, E. and Chua, K.F. (2010) Functional dissection of SIRT6: identification of domains that regulate histone deacetylase activity and chromatin localization. *Mech Ageing Dev*, **131**, 185-192.
27. Wang, D., Kon, N., Lasso, G., Jiang, L., Leng, W., Zhu, W.-G., Qin, J., Honig, B. and Gu, W. (2016) Acetylation-regulated interaction between p53 and SET reveals a widespread regulatory mode. *Nature*, **538**, 118-122.
28. Hu, S., Pluth, J.M. and Cucinotta, F.A. (2012) Putative binding modes of Ku70-SAP domain with double strand DNA: a molecular modeling study. *J Mol Model*, **18**, 2163-2174.
29. Tang, X., Shi, L., Xie, N., Liu, Z., Qian, M., Meng, F., Xu, Q., Zhou, M., Cao, X., Zhu, W.-G. *et al.* (2017) SIRT7 antagonizes TGF-β signaling and inhibits breast cancer metastasis. *Nature Communications*, **8**, 318.
30. Soutoglou, E., Dorn, J.F., Sengupta, K., Jasin, M., Nussenzweig, A., Ried, T., Danuser, G. and Misteli, T. (2007) Positional stability of single double-strand breaks in mammalian cells. *Nature Cell Biology*, **9**, 675.
31. Rogakou, E.P., Pilch, D.R., Orr, A.H., Ivanova, V.S. and Bonner, W.M. (1998) DNA double-stranded breaks induce histone H2AX phosphorylation on serine 139. *The Journal of biological chemistry*, **273**, 5858-5868.
32. Paull, T.T. and Lee, J.H. (2005) The Mre11/Rad50/Nbs1 complex and its role as a DNA double-strand break sensor for ATM. *Cell Cycle*, **4**, 737-740.
33. Marechal, A. and Zou, L. (2015) RPA-coated single-stranded DNA as a platform for post-translational modifications in the DNA damage response. *Cell Res*, **25**, 9-23.
34. Ali, A.A.E., Timinszky, G., Arribas-Bosacoma, R., Kozlowski, M., Hassa, P.O., Hassler, M., Ladurner, A.G., Pearl, L.H. and Oliver, A.W. (2012) The zinc-finger domains of PARP1 cooperate to recognize DNA strand breaks. *Nat Struct Mol Biol*, **19**, 685-692.
35. Eustermann, S., Wu, W.F., Langelier, M.F., Yang, J.C., Easton, L.E., Riccio, A.A., Pascal, J.M. and Neuhaus, D. (2015) Structural Basis of Detection and Signaling of DNA Single-Strand Breaks by Human PARP-1. *Mol Cell*, **60**, 742-754.
36. Yang, G., Liu, C., Chen, S.H., Kassab, M.A., Hoff, J.D., Walter, N.G. and Yu, X. (2018) Super-resolution imaging identifies PARP1 and the Ku complex acting as DNA double-strand break sensors. *Nucleic Acids Res*.
37. Malik, S., Villanova, L., Tanaka, S., Aonuma, M., Roy, N., Berber, E., Pollack, J.R., Michishita-Kioi, E. and Chua, K.F. (2015) SIRT7 inactivation reverses metastatic phenotypes in epithelial and mesenchymal tumors. *Scientific Reports*, **5**.
38. Fang, J., Ianni, A., Smolka, C., Vakhrusheva, O., Nolte, H., Kruger, M., Wietelmann,

A., Simonet, N.G., Adrian-Segarra, J.M., Vaquero, A. *et al.* (2017) Sirt7 promotes adipogenesis in the mouse by inhibiting autocatalytic activation of Sirt1. *Proc Natl Acad Sci U S A*.

39. Tjeertes, J.V., Miller, K.M. and Jackson, S.P. (2009) Screen for DNA-damage-responsive histone modifications identifies H3K9Ac and H3K56Ac in human cells. *EMBO J*, **28**, 1878-1889.
40. Atsumi, Y., Minakawa, Y., Ono, M., Dobashi, S., Shinohe, K., Shinohara, A., Takeda, S., Takagi, M., Takamatsu, N. and Nakagama, H. ATM and SIRT6/SNF2H Mediate Transient H2AX Stabilization When DSBs Form by Blocking HUWE1 to Allow Efficient gH2AX Foci Formation.
41. Olive, P.L. and Banáth, J.P. (2006) The comet assay: a method to measure DNA damage in individual cells. *Nature Protocols*, **1**, 23.
42. Falck, J., Coates, J. and Jackson, S.P. (2005) Conserved modes of recruitment of ATM, ATR and DNA-PKcs to sites of DNA damage. *Nature*, **434**, 605.